Analytical Derivation of Controller Parameters for Series Connected LCC Multiterminal HVDC Systems through the use of a Decoupling Filter

Stefan Hammer[1], Christoph Hahn[2], *Member*, *IEEE*, Matthias Luther[2], *Member, IEEE*
[1]Siemens AG
[2]Friedrich-Alexander-University of Erlangen-Nuremberg (FAU)
Institute of Electrical Energy Systems
Erlangen, Germany
stefanhammer@siemens.com, christoph.hahn@fau.de, matthias.luther@fau.de

Abstract – This paper demonstrates the design process of a decoupled control for any series connected Line-Commutated Converter (LCC) Multiterminal (MT) High-Voltage Direct Current (HVDC) system. After the introduction of a modular average model, devoid of the typical current converter switching behavior, a structured mathematical description as a Multiple-Input-Multiple-Output-system (MIMO) is presented. This facilitates the calculation of a decoupling filter and enables the analytical derivation of PI-controller parameters. For that purpose, an approach using Amplitude Optimum was chosen. Compared to a conventional control design, the sophisticated method clearly shows improvement of operational behavior and stability of an Electro-Magnetic-Transient (EMT) model.

Keywords – Amplitude Optimum, Decoupled Control, HVDC Control, HVDC Modelling, LCC HVDC, Multiterminal HVDC

I. INTRODUCTION

For several decades now, HVDC transmissions are used in conjunction with conventional three-phase AC-systems for various economic and technical reasons: They enable the interconnection of power grids which would otherwise be incompatible (e.g. due to different and asynchronous frequencies), they offer a reduction in transmission losses for long distance bulk power transmissions and for cable links that extend over more than about 80km there is no alternative. [1] Additionally, they also facilitate a fast and precise control of power flow, a merit with increasingly volatile feed-in.

There are two different HVDC converter technologies currently available: The newer Voltage Sourced-Converter (VSC) systems which are IGBT-based, have attracted research attention in the recent years and first experiences in operation are now being made. The other, more robust LCC Converters have already proven to be a reliable investment through long-standing experience in operation. Whilst the very first versions of LCC-type converters were implemented as mercury arc valves, advancement in semiconductor technology in the seventies established the use of silicon thyristors, which since then has become the prevailing technology. Elaborate description of the conventional HVDC system can be found in literature (e.g. [2]). A LCC can operate as rectifier or inverter and consists of one or more six-pulse bridges connected to the three-phase AC-grid with or without a 30° phase shift. The DC-voltage can be adjusted by changing the thyristor ignition angle α. As thyristors conduct only in forward direction, a reversal of power flow does require a voltage inversion. LCC configurations can be mono- or bipolar. Typically, the rectifier is controlling the DC-current and the inverter is in voltage or extinction angle control mode. [3] Mainly, empirically parametrized PI-Controllers are utilized as outlined e.g. in [4] and [5].

With the ongoing shift of power generation towards renewable energy sources, such as solar power, wind and biomass, Transmission System Operators (TSOs) worldwide are challenged to rethink their grid structures. In Germany, TSOs and the Federal Network Agency (BNetzA) are already coordinating their efforts to adapt: HVDC links will be key components to ensure network stability and transport renewable generated power from north to south [6]. Even more sophisticated grid structures such as an overlying multi-terminal DC-system could be a reasonable future extension. [7] Basically, there are three possible ways to interconnect AC/DC converter stations: serial, parallel or mashed. [1] In terms of control, all variants can be seen as MIMO systems. This paper will demonstrate how to form a decoupling filter by using a mathematical model, which does not contain the current converter switching frequency components. The MIMO-system thereby is reduced to several single-input single-output systems. This allows the analytical derivation of control parameters. An underlying necessity for this approach is a fast communication between every station. A decoupling approach that linearized the system transfer function at a certain operating point and utilized a controller parametrization in frequency domain using the bode diagram was carried out in [8].

II. A MODULAR AVERAGE MODEL

A modular average model is derived using the following approach: Through space phasor transformation and phasor rotations (for detailed explanations refer to [9] and [10]), a HVDC transmission is separated into subsystems. Each subsystem is formed out of a six-pulse bridge with its dedicated source. If two subsystems are connected on the AC-side (e.g. in form of a twelve-pulse bridge), the influence of the shared impedance (AC-network impedance and primary side transformer impedance) is increased. Fig. 1 indicates this modular concept.

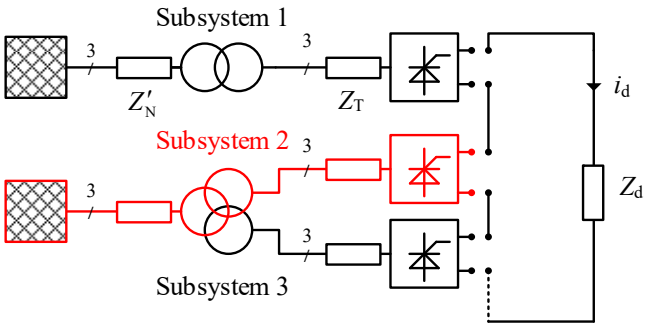

Fig. 1: Separating a HVDC transmission into subsystems

This yields a simple generalized equivalent circuit that – ensuing the calculation of arithmetic mean values of one converter period $T/6$ – is depicted in Fig. 2. It consists of a DC-voltage source $\overline{v}$ and an impedance $\overline{Z}$.

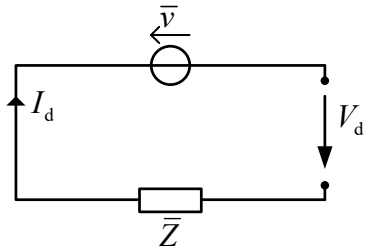

Fig. 2: Equivalent circuit of one subsystem (average model)

The average value of the DC-voltage $\overline{v}$ is dependent on the ignition angle and AC-voltage. Also, as a higher DC-current I_d or an increase in the AC-side inductances prolongs the commutation, they both reduce the effective DC-voltage:

$$\overline{v} = \frac{3\cdot\sqrt{2}}{\pi}\cdot V_{AC,sec}\cdot\cos(\alpha) - \frac{3}{\pi}\cdot(X_N + X_T)\cdot I_d. \quad (1)$$

For steady-state considerations this term can be used to calculate the terminal DC-voltage V_d in good approximation. However, this is not entirely correct, as it misrepresents the influence of AC-side impedances especially regarding dynamic behavior. For a six-pulse bridge the effective mean impedance $\overline{Z}$ is given in (2), whilst for a twelve-pulse bridge it is determined according to (3), as the shared impedance Z_N then contributes with the factor $k+\sqrt{3}$:

$$\overline{Z} = K\cdot(Z_T + Z_N), \quad (2)$$

$$\overline{Z} = K\cdot(Z_T + Z_N) + \sqrt{3}Z_N. \quad (3)$$

It shall be noted that the factor K was chosen as an approximation for the derivation of the average value:

$$K = \frac{K_{TVC} + K_{COM}}{2} = \frac{2+\frac{3}{2}}{2} \approx 1.8. \quad (4)$$

Moreover, K is dependent on the extinction angle as during two-vales conduction, the AC-side impedances effectively contribute with a factor of 2, whereas during commutation, their influence reduces to the factor 1.5. A description of the relevant parameters is given in Table 1. To maintain comprehensibility a simple two-subsystems HVDC will now serve as an example. Providing a decoupling filter and deriving PI-controller parameters shall be demonstrated step by step.

Table 1: Equivalent circuit parameters

$Z_N = R_N + s\cdot L_N$	All impedances belonging to the transformer primary side referred to the secondary side. This is mainly the short circuit impedance of the AC-system (*RL*-Thévenin equivalent).
$Z_T = R_T + s\cdot L_T$	All transformer secondary side impedances. This is mainly the short circuit impedance of the transformer.
$V_{AC,sec}$	Phase-to-phase RMS-value of the ideal symmetrical three-phase AC-voltages referred to the secondary side.

III. THE MIMO-SYSTEM TRANSFER FUNCTION

The corresponding average model is depicted as a block diagram in Fig. 3. It visualizes the relation between the system output variables I_d, and $V_{d,2}$ and the control variables $\cos(\alpha_1)$ and $\cos(\alpha_2)$. An impedance Z_d was included to represent smoothing reactors and the DC-line impedance.

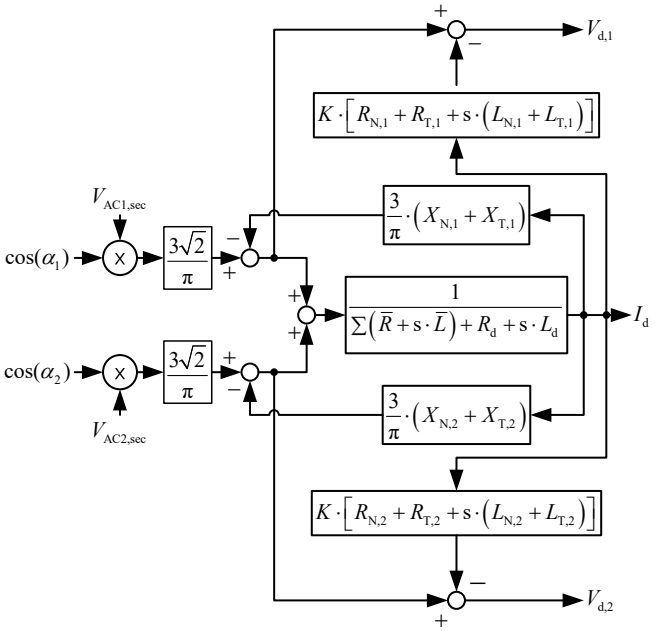

Fig. 3: Block diagram of a two-subsystems HVDC transmission

To simplify this structure, substitutions T_{id} (5), K_{id} (6), $T_{vd,2}$ (7) and $K_{vd,2}$ (8) are introduced and equations (9) and (10) can be carried out.

$$T_{id} = \frac{L_d + K\cdot(L_{N,1}+L_{T,1}+L_{N,2}+L_{T,2})}{\left[\begin{array}{l}\frac{3}{\pi}\cdot(X_{N,1}+X_{T,1}+X_{N,2}+X_{T,2})+R_d+\\ +K\cdot(R_{N,1}+R_{T,1}+R_{N,2}+R_{T,2})\end{array}\right]} \quad (5)$$

$$K_{id} = \frac{\frac{3\sqrt{2}}{\pi}}{\left[\begin{array}{l}\frac{3}{\pi}\cdot(X_{N,1}+X_{T,1}+X_{N,2}+X_{T,2})+R_d+\\ +K\cdot(R_{N,1}+R_{T,1}+R_{N,2}+R_{T,2})\end{array}\right]} \quad (6)$$

$$T_{vd,2} = K\cdot(L_{N,2}+L_{T,2}) \quad (7)$$

$$K_{\mathrm{vd,2}} = \left(\frac{3}{\pi} \cdot \left(X_{\mathrm{N,2}} + X_{\mathrm{T,2}} \right) + K \cdot \left(R_{\mathrm{N,2}} + R_{\mathrm{T,2}} \right) \right) \tag{8}$$

$$\begin{aligned} I_{\mathrm{d}} = {} & \cos(\alpha_1) \cdot \underbrace{V_{\mathrm{AC1,sec}} \cdot \frac{K_{\mathrm{id}}}{1 + T_{\mathrm{id}} \cdot \mathrm{s}}}_{G_{11}} + \\ & + \cos(\alpha_2) \cdot \underbrace{V_{\mathrm{AC2,sec}} \cdot \frac{K_{\mathrm{id}}}{1 + T_{\mathrm{id}} \cdot \mathrm{s}}}_{G_{12}} \end{aligned} \tag{9}$$

$$\begin{aligned} V_{\mathrm{d,2}} = {} & \cos(\alpha_1) \cdot \underbrace{V_{\mathrm{AC1,sec}} \cdot \frac{-K_{\mathrm{id}} \cdot \left(K_{\mathrm{vd,2}} + \mathrm{s} \cdot T_{\mathrm{vd,2}} \right)}{1 + T_{\mathrm{id}} \cdot \mathrm{s}}}_{G_{21}} + \\ & + \cos(\alpha_2) \cdot \underbrace{V_{\mathrm{AC2,sec}} \cdot \left(\frac{3\sqrt{2}}{\pi} - \frac{K_{\mathrm{id}} \cdot \left(K_{\mathrm{vd,2}} + \mathrm{s} \cdot T_{\mathrm{vd,2}} \right)}{1 + T_{\mathrm{id}} \cdot \mathrm{s}} \right)}_{G_{22}} \end{aligned} \tag{10}$$

As indicated, this rearrangement yields a compressed, structured description represented by the system transfer matrix **G**(s):

$$\begin{pmatrix} I_{\mathrm{d}}(s) \\ V_{\mathrm{d2}}(\mathrm{s}) \end{pmatrix} = \begin{pmatrix} G_{11} & G_{12} \\ G_{21} & G_{22} \end{pmatrix} \begin{pmatrix} \cos(\alpha_1) \\ \cos(\alpha_2) \end{pmatrix}. \tag{11}$$

IV. DECOUPLING & CONTROLLER PARAMETRIZATION

In order to perform an analytical controller parametrization for a MIMO system there are two options: designing a control in state space or decoupling the multi variable system and then applying conventional parametrization techniques. The latter shall be demonstrated. Fig. 4 visualizes the desired effect of the so called decoupling filter matrix **F**(s): Compensation of the unwanted influence of secondary diagonal elements of the system transfer function, in this case G_{12} and G_{21}.

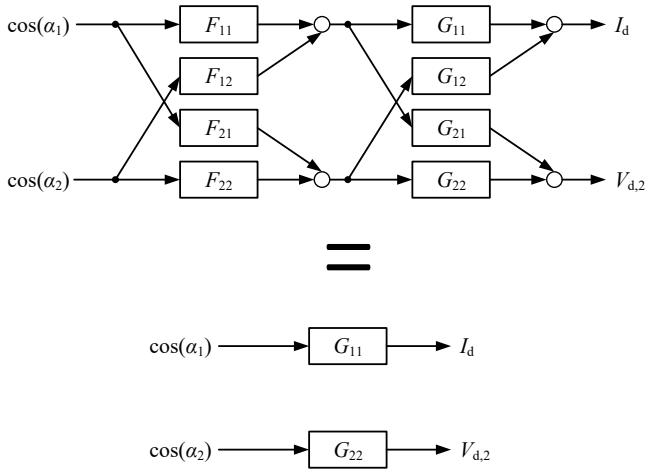

Fig. 4: Decoupling scheme

This can also be described by means of an equation system:

$$\begin{aligned} F_{12} \cdot G_{11} + F_{22} \cdot G_{12} &= 0, \\ F_{21} \cdot G_{22} + F_{11} \cdot G_{21} &= 0, \\ F_{21} \cdot G_{12} + F_{11} \cdot G_{11} &= G_{11}, \\ F_{12} \cdot G_{21} + F_{22} \cdot G_{22} &= G_{22}. \end{aligned} \tag{12}$$

By solving (11) the four filter matrix elements F_{11}, F_{12}, F_{21} and F_{22} can be derived:

$$\begin{aligned} F_{11} &= \frac{G_{11} G_{22}}{G_{11} G_{22} - G_{21} G_{12}}, \; F_{12} = \frac{G_{11} G_{22} G_{12}}{G_{21} G_{12} G_{11} - G_{22} G_{11} G_{11}}, \\ F_{21} &= \frac{G_{11} G_{22} G_{21}}{G_{21} G_{12} G_{22} - G_{11} G_{22} G_{22}}, \; F_{22} = \frac{G_{11} G_{22}}{G_{22} G_{11} - G_{21} G_{12}}. \end{aligned} \tag{13}$$

Fig. 5 shows the average model block diagram of the entire control system. It was unnecessary to include ignition angle delay and limitation into the system transfer function **G**(s) for the calculation of the decoupling matrix since it has no influence on the equation system. The average dead time (13) was found through the following consideration: If a change of the ignition angle α happens right after thyristor ignition, it will take 60°+$\Delta\alpha$ to effect the system. If a change of α happens right before thyristor ignition it will take $\Delta\alpha$ for the change to manifest. A delay first order as a Taylor-approximation of a dead time element was used.

$$T_{\mathrm{d}} = \frac{\left(60° + \Delta\alpha\right) - \Delta\alpha}{2} \frac{\mathrm{T}}{360°} = \frac{30°}{360°} \cdot \mathrm{T} \tag{14}$$

Additionally, a smoothing of the DC-voltage measurement $V_{\mathrm{d,2}}$ was included, such an element is used in reality to mitigate the typical six pulse voltage ripple.

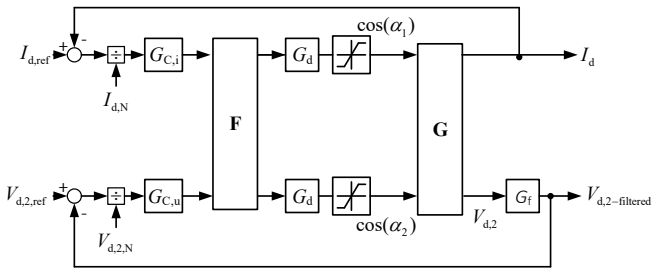

Fig. 5: Full average model

Controller parameters shall now be derived in time domain. The Objective is an improvement of transient system behavior. $\cos(\alpha_1)$ will be used for current control, the corresponding open loop transfer function is:

$$G_{\mathrm{o}} = \underbrace{\frac{1}{I_{\mathrm{d,N}}}}_{\text{normalizing}} \cdot \underbrace{V_{\mathrm{R}} \frac{1 + \mathrm{s} T_{\mathrm{N}}}{\mathrm{s} \cdot T_{\mathrm{N}}}}_{\text{PI-current controller}} \cdot \underbrace{\frac{1}{1 + T_{\mathrm{d}} \cdot \mathrm{s}}}_{\text{ignition angle delay}} \cdot \underbrace{\frac{V_{\mathrm{AC1,sec}} \cdot K_{\mathrm{id}}}{1 + T_{\mathrm{id}} \cdot \mathrm{s}}}_{\text{effective system}} \tag{15}$$

Using the approach of Amplitude Optimum, the dominant time constant of the system is supposed to be compensated by the time constant T_{N} of the PI-controller, since the ignition angle delay T_{d} is a non-compensable time constant anyway:

$$T_{\mathrm{N}} \coloneqq T_{\mathrm{id}}. \tag{16}$$

The open loop transfer function is thereby reduced to:

$$G_{\mathrm{o}} = \frac{V_{\mathrm{R}} \cdot \frac{1}{I_{\mathrm{d,N}}} \cdot V_{\mathrm{AC1,sec}} \cdot K_{\mathrm{id}}}{\mathrm{s} \cdot T_{\mathrm{id}}} \cdot \frac{1}{1 + T_{\mathrm{d}} \cdot \mathrm{s}}. \tag{17}$$

The transfer function of the closed loop is a second order delay, which can be rewritten in a standardized form:

$$G_W = \frac{1}{\frac{T_d \cdot T_{id}}{V_R \cdot \frac{1}{I_{d,N}} \cdot V_{AC1,sec} \cdot K_{id}} \cdot s^2 + \frac{T_{id}}{V_R \cdot \frac{1}{I_{d,N}} \cdot V_{AC1,sec} \cdot K_{id}} \cdot s + 1} = \frac{1}{\frac{1}{\omega^2} \cdot s^2 + \frac{2D}{\omega} \cdot s + 1}. \quad (18)$$

Amplitude Optimum definition demands that the frequency response of the closed loop transfer function contains no resonant peak. [11] The damping D consequently yields:

$$D = \frac{1}{\sqrt{2}}. \quad (19)$$

By comparing coefficients, the controller gain V_R is found:

$$V_R := \frac{T_{id}}{T_d \cdot 2 \cdot V_{AC1,sec} \cdot \frac{1}{I_{d,N}} \cdot K_{id}}. \quad (20)$$

$\cos(\alpha_2)$ shall be used for voltage control. Its open loop transfer function is:

$$G_o = \frac{1}{V_{d,2,N}} \cdot V_R \frac{1 + sT_N}{sT_N} \cdot \frac{1}{1 + T_d \cdot s} \cdot V_{AC2,sec} \cdot \left[\frac{3\sqrt{2}}{\pi} - \frac{K_{id} \cdot \left(K_{vd,2} + s \cdot T_{vd,2} \right)}{1 + T_{id} \cdot s} \right] \cdot \frac{1}{1 + T_f \cdot s}. \quad (21)$$

As amplitude Optimum is only suitable for lag element and integral element systems the differential part in (21) will be neglected for the following considerations. Again, the dominant time constant of the system is compensated by T_N of the PI-controller:

$$T_N := T_{id}. \quad (22)$$

After applying the Amplitude Optimum approach to the voltage controller, the gain can be determined as well:

$$V_R := \frac{T_{id}}{\left(T_d + T_f \right) \cdot 2 \cdot \frac{1}{V_{d,2,N}} \cdot V_{AC2,sec} \cdot \frac{3\sqrt{2} - K_{vd,2} K_{id} \cdot \pi}{\pi}}. \quad (23)$$

V. RESULTS

To proof accuracy and examine behavior of the controlled system, an average model and an EMT model were built in MATLAB® Simulink. The system configuration and appropriate parameters are shown with Fig. 6.

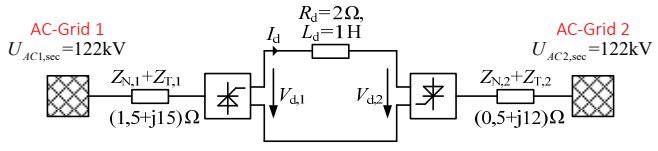

Fig. 6: System configuration

A classical non-decoupled empirically parametrized PI-control was implemented as a benchmark. Controller parameters for the decoupled control were calculated according to Chapter V. The desired value $I_{d\text{-ref}}$ was changed six times in different steps. $V_{d,2\text{-ref}}$ was permanently set to 100 kV. Fig. 7 shows that an overshoot during the adjustment to a new value is not avoided when using the non-decoupled control; furthermore, any change of I_d quite noticeably influences $V_{d,2}$.

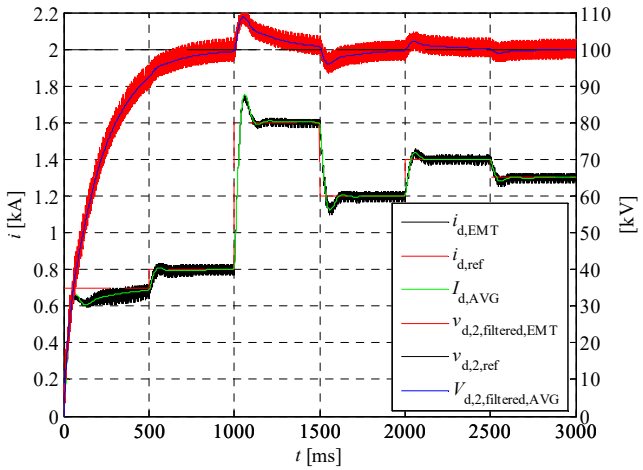

Fig. 7: DC-current and voltage step response: classical control using both EMT and average model

Fig. 8 shows simulation results using the decoupled control; the adjustment to a new desired value has highly improved: It is faster, without an overshoot and does not influence $V_{d,2}$. Due to the non-linear effect of the ignition angle limitation – which prevented an ideal control behavior during the +800 A step at t=1000 ms – controller gain values were reduced.

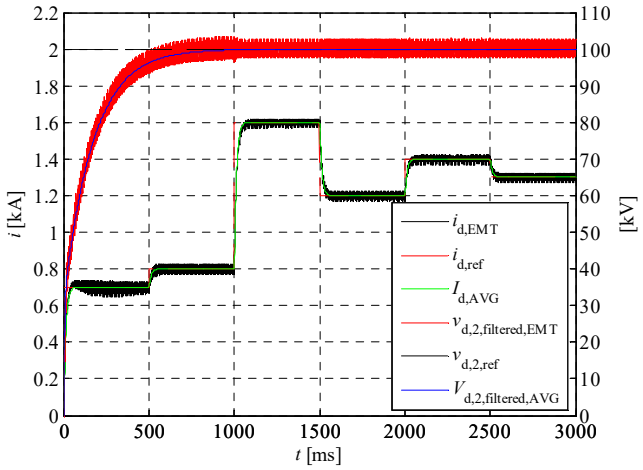

Fig. 8: DC-current and voltage step response: decoupled control using both EMT and average model

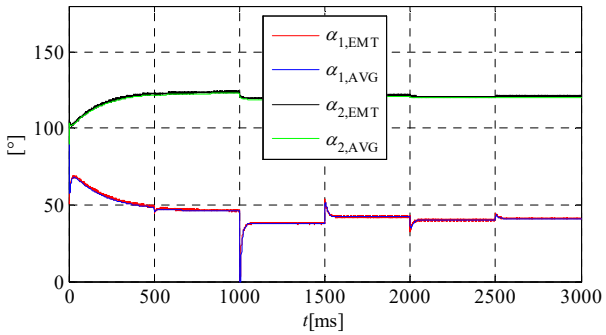

Fig. 9: Ignition angles: decoupled control using both EMT and average model

As mentioned, the outlined approach is suitable for any serially connected HVDC system. For further investigations a HVDC configuration with three subsystems was decoupled and controller parameters were determined according to the presented method. Fig. 10 shows the decoupling scheme. As the number of the defining equations is proportional to the square of the number of subsystems, a symbolic solver (the MATLAB® Symbolic Math Toolbox) was used to facilitate the calculation of the individual matrix elements.

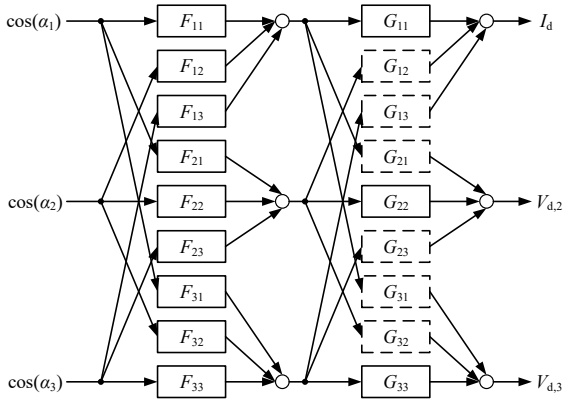

Fig. 10: Decoupling scheme: The filter elements are determined to compensate the secondary diagonal elements; subsystem 1 is in current control mode, subsystem 2 and 3 are in voltage control mode

Fig. 11 shows simulation results for a three-subsystems HVDC, proving a sucessfully decoupled system behaviour. System and controller parameters are given in Table 2 and Table 3.

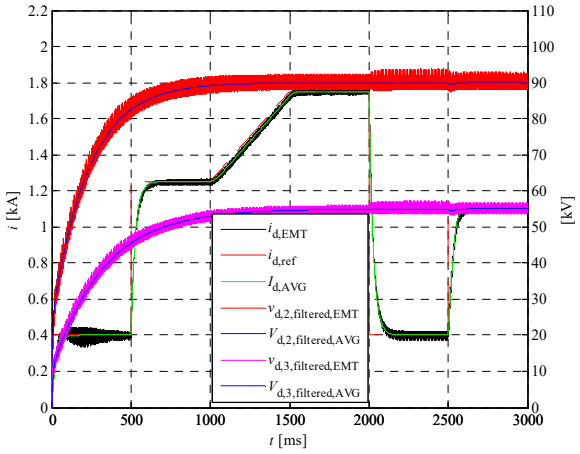

Fig. 11: DC-current and voltages for a three-subsystems HVDC

Table 2: Controller parameters for a three-subsystems HVDC

	V_R	T_N
I_d	$\frac{T_{id}}{T_d \cdot 2 \cdot V_{AC1,sec} \cdot \frac{1}{I_{d,N}} \cdot K_{id}}$	T_{id}
$V_{d,2}$	$\frac{T_{id}}{(T_d + T_f) \cdot 2 \cdot \frac{1}{V_{d,2,N}} \cdot V_{AC2,sec} \cdot \frac{3\sqrt{2} - K_{vd,2} K_{id} \cdot \pi}{\pi}}$	T_{id}
$V_{d,3}$	$\frac{T_{id}}{(T_d + T_f) \cdot 2 \cdot \frac{1}{V_{d,3,N}} \cdot V_{AC3,sec} \cdot \frac{3\sqrt{2} - K_{vd,3} K_{id} \cdot \pi}{\pi}}$	T_{id}

Table 3: System parameters of a three-subsystems HVDC

$f_{N1}=f_{N2}=f_{N3}$	50 Hz	$R_d \mid L_d$	2 Ω | 1H
$V_{AC1,sec}$	100 kV	$Z_{N1} + Z_{T1}$	(0.75+7.5j) Ω
$V_{AC2,sec}$	80 kV	$Z_{N2} + Z_{T2}$	(0.25+6j) Ω
$V_{AC3,sec}$	50 kV	$Z_{N3} + Z_{T3}$	(0.5+5j) Ω

VI. CONCLUSION

This paper presents an approach of modelling and control design for any serially connected HVDC system. It is based on the reduction of the MIMO system to several single-input single-output systems using a decoupling filter. Hence, classical control theory methods for the analytical derivation of parameters can be applied. In this case the approach of Amplitude Optimum was investigated. Compared to a conventional control, this method shows several advantages:

- Unwanted interaction between the different controllers is diminished, as changing the desired value of one controller does no longer influence the other converters.
- Control behavior in general is much closer to an ideal performance as the adjustment to new desired values is faster and without an overshoot.
- Control parametrization can be done analytically instead of empirically. If for any considered scenario the ignition angle limitation interferes with an ideal control behavior, the analytically derived values can still serve as a good point of reference.

REFERENCES

[1] V. Crastan and D. Westermann, Electrical Power Supply III (Elektrische Energieversorgung III), Berlin Heidelberg, Germany: Springer publishing, 2012.

[2] E. W. Kimbark, Direct Current Transmission, New York, USA: John Wiley & Sons, 1971.

[3] K.-W. Kanngießer, HVDC Systems and their Planning, Munich, Germany: Siemens, 1996.

[4] F. Yang and Z. Xu, "An approach to Select PI Parameters of HVDC Controllers," in *IEEE PES General Meeting*, Montreal, Canada, June 2006.

[5] A. E. Hammad, "Stability and Control of HVDC and AC Transmissions in Parallel," *IEEE Transactions on Power Delivery,* Vol. 14, No. 4, October 1999.

[6] 50Hz, Amprion, TenneT and TransnetBW, German grid development plan 2025 (Netzentwicklungsplan Strom 2025), Germany: German Transmission System Operators, 2015.

[7] S. Cole, K. Karoui, T. Vrana and O. Fosso, "A European Supergrid: Present State And Future Challenges," in *17th Power Systems Computation Conference*, Stockholm, Sweden, August 2011.

[8] C. Hahn, A. Müller and M. Luther, "A novel approach to select HVDC - controller parameters by using a decoupling filter," in *International Conference on Renewable Energies and Power Quality*, Bilbao, Spain, March 2013.

[9] G. Herold, Electrical Energy Supply V: Current Converters in Three-Phase AC-Systems (Elektrische Energieversorgung V: Stromrichter in Drehstromnetzen), Wilburgstetten: Schlembach Fachverlag, 2009.

[10] L. Probst, C. Hahn and M. Luther, "A Novel Approach for Analytical Modeling of Line Commutated Converter based HVDC Systems for Electromagnetic Transient Analysis," in *IEEE PowerTech*, Eindhoven, June 2015.

[11] O. Föllinger, Control Engineering (Regelungstechnik), Heidelberg, Germany: Hüthig publishing, 1994.